

Echoic Flow for Guidance and Control

Graeme E. Smith and Chris J. Baker

The Ohio State University

USA

ABSTRACT

In these lecture notes the role of cognitive radar for guidance and control is discussed. The theory of echoic flow is introduced as a method by which the environmental parameters measured by radar may be converted into a perception from which motion actions may be deduced. Indeed, such is the utility of echoic flow that it provides a way to determine the actions as well as a way to form the perception. However, the role of cognition for radar is not limited to guidance and control. In the second part of the notes a consideration is given to how cognition can support the selection of radar parameters in a tracking example. This use of cognition provides a paradigm shift in the way an operator interacts with the radar. Rather than have an operator select parameters based on anticipated targets, the operator now specifies the level of performance required and the cognitive radar selects the parameters necessary to meet the specified performance.

I INTRODUCTION

The application of cognitive-like processing to radar is a fast emerging area of research that has the potential to influence almost all types of radar sensing systems. Cognition means ‘knowing’ and is the process by which humans know about the world. In the simplest of terms, cognitive radar can be thought of as a system of hardware and software that is able to adaptively adjust transmit and receive parameters in real-time to optimize performance for a given application. This leads directly to the concept of the perception-action cycle as described in [1], [2]. Further and consistent with models of cognition, any current perception forms the basis of future memories and these, along with past memories, can be used intelligently to aid perception, apply attention and to form predictions as part of future task planning and execution. It is this notion of the perception-action cycle, generating and exploiting memories, the presence of intelligence and use of attention that forms the core of our approach to cognitive radar sensing.

It is also prudent to consider bio-inspired techniques alongside cognition since these techniques often provide a framing for the problem that supports cognition. Here we consider the concept of echoic flow [3]–[5] as a method to combine the range and velocity information measured by a radar sensor. The more general flow theory has been shown capable of describing a vast array of natural control problems [6]–[8] and echoic flow is the instantiation of this theory for echolocating sensors. Lee *et al.* have provided compelling evidence that bats utilise flow theory [6] and their approach will be used in the explanation of echoic flow theory provided here.

This paper will discuss the theory of echoic flow in Section II and discuss how it can facilitate cognitive processing. Section III will report how cognition can be applied to radar to enable the operator to specify performance and the system then adapt its parameters to meet this performance. Conclusions will be drawn in Section IV.

II FLOW FIELDS FOR COGNITIVE GUIDANCE AND CONTROL

II.A Overview of Echoic Flow

Bats provide an excellent example of a natural echolocating cognitive system. They sense the environment by transmitting “calls” collimated in a beam which can be directed into the surrounding open space. Echoes are processed on reception in both ears. Bats are able to perceive their environment such that they can navigate, avoid collisions, select targets and make decisions critical to their survival. They do this by adapting to the characteristics of the environment and continuously changing their echolocation sensing parameters such as the form of the call (frequency and depth and rate of modulation), call duration, the rate at which calls are transmitted, call amplitude and the direction in which the call is transmitted, e.g. [9], [10]. This section explores methods and strategies for collision-free guidance and orientation based on exploiting echoic flow fields.

Flow fields were first conceived by Gibson [11] and subsequently developed by Lee and co-workers, e.g. [8] Flow field theory seeks to explain how humans and other members of the animal kingdom are able to navigate complex environments without having to compute and re-compute the position of all objects and obstacles along with the position of self. Flow fields naturally occur in many domains but most research attention has been on vision in the form of optical flow, see [12] and references therein. Optical flow represents the relative movement between a point of observation and objects in an illuminated environment as the ratio of light intensity to changes in light intensity. A human walking towards a doorway will exploit observed changes in the global pattern of scattered light. The instantaneous time to reach the doorway is automatically sensed and the nervous system controls the approach to, and transit through, the doorway.

Flow fields are a direct measure of the time for objects in relative motion to come together or, more generally, for a gap to be closed. The closure of a gap includes, for example, the closure of the angle between a current or reference direction of travel and a desired direction of travel. Distance and angle gaps can be combined enabling the computation of three-dimension flow fields. The derivative of a flow field determines how the gap will be closed. Holding the derivative at a constant value fixes the form of the resulting trajectory. A range of trajectory types can be chosen by selecting the value of the constant thus enabling different types of task to be carried out. Crucially, the sensed flow field (perception) can be used to directly compute the desired trajectory (action) consistent with [7]. In the case of humans a neuronal response stimulates muscles in the required way. Therefore measurement of gap closure times in both distance and angle (azimuth and elevation) provides a powerful basis for enabling autonomous behaviors in synthetic systems. The flow field or gap closure time is usually denoted with the parameter τ and this convention will be adopted here.

Bats have been shown [6] to perform tasks such as intercepting prey on the wing or maneuvering to a landing site in a manner that is consistent with exploitation of flow fields. Lee uses the term acoustic flow whereas here the term echoic flow (EF) is employed to specifically denote an active sensing system where acoustic or electromagnetic signals are transmitted and received. In [6] it is concluded that bats use EF as a method enabling controlled landings and feeding on the wing. The behavior of the bat was found to be consistent with computation of EF and its derivative in both range and angle. Bats employ a strategy whereby the values of the derivatives of range and angle EF take a specific value. Radar and sonar systems inherently measure distance and angle using echolocation and thus lend themselves well to the measurement of 3-D flow fields. The flow field, τ , associated with radial range is given by:

$$\tau_r = r / \dot{r} \quad (1)$$

where r is the range to a detected object and \dot{r} is the change in range of the object between the current and previous measurements. Strictly τ_r , r and \dot{r} are all functions of time, t , however, here the ‘(t)’ has been omitted for clarity in the equations.

τ_r is a direct measure of the time to collision or time to close the range gap and has units of time. For example, if a radar sensor system is moving directly towards a stationary object with a velocity of 3 ms^{-1} and the object is located at a distance of 6 m, the gap closure time is 2 s.

The time derivative of τ , denoted $\dot{\tau}$, is a dimensionless quantity that is related to the velocity and acceleration as the system approaches a target. $\dot{\tau}$ depends on range, range rate and acceleration according to:

$$\dot{\tau}_r = \frac{\partial \tau_r}{\partial t} = 1 - \frac{r\ddot{r}}{\dot{r}^2} = 1 - \tau_r \frac{\ddot{r}}{\dot{r}} \quad (2)$$

Equation (2) is a second order differential equation and can be solved for cases where $\dot{\tau}$ takes a constant value, k , to give the expression in (3a) that describes the change in range as a function of time and the initial range and echoic flow. Differentiating (3a) with respect to time gives (3b) that describes the progression of range-rate, or speed. A further differentiation gives (3c) that describes the progression of acceleration. Equations (3a) to (3c) are the equations of motion for the system [3], [6]:

$$r = r_0 \left(1 + kt/\tau_0\right)^{\frac{1}{k}} \quad (3a)$$

$$\dot{r} = \dot{r}_0 \left(1 + kt/\tau_0\right)^{\frac{1}{k}-1} \quad (3b)$$

$$\ddot{r} = \left(\dot{r}_0^2/r_0\right) (1 - k) \left(1 + kt/\tau_0\right)^{\frac{1}{k}-2} \quad (3c)$$

where r_0 and \dot{r}_0 are the range and velocity at $t = 0$ and $\tau_0 = r_0/\dot{r}_0$ is the initial echoic flow. The convention is that the initial range is negative while the velocity is positive, i.e. the gap between radar platform and target is closing. These are the basic equations of EF and, as shown here, enable the sensed flow field to generate changes to velocity and acceleration such that a desired trajectory is followed. Note that the range, r , in (3) could be replaced with any sensor measurable parameter permitting its control by echoic flow.

Fig. 1 shows the equation of motion curves, for constant values of $\dot{\tau}_r = k$ and initial conditions of $r_0 = -10 \text{ m}$ and $\dot{r}_0 = 1 \text{ ms}^{-1}$. In this example, the radar is part of a vehicle approaching the object head-on. Unless braking is applied the vehicle and object will collide. Fig. 1 shows five regions of behavior types.

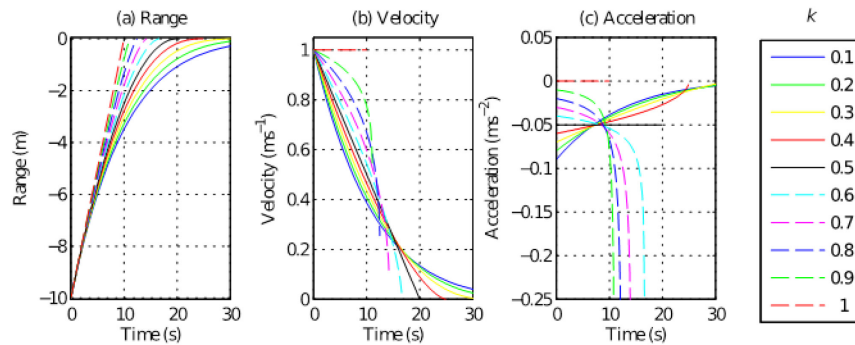


Fig. 1: The variation, over time, of (a) range, (b) velocity and (c) acceleration as the sensor system approaches a target. Note the accelerations are negative indicating braking. Curves are calculated using (3).

- 1) $k = 1$. There is no change in acceleration with time and the platform collides with the target after 10 s at the same speed as when the target was first detected. The collision is “hard”.
- 2) $0.5 < k < 1$. The trajectory is consistent with “a late braking strategy” (such as one might be used by a runner in baseball). This still results in a collision as the sensor platform vehicle still has positive velocity. However, the initial braking acceleration (with negative value) is insufficient to stop the system at the object location. As the sensor platform approaches the target the braking increases (theoretically to an infinite amount) at the instant the vehicle and object collide. Infinite braking would mean there is no actual collision with the target, since the velocity will become zero at zero gap. However, no real system (or baseball runner) can actually have a negative infinite acceleration, so in practice the platform will crash into the target with a positive velocity and the collision can still be hard, depending on the value of k .
- 3) $0 < k < 0.5$. This is an example of an early braking strategy (such as one might be used by the driver of a passenger vehicle). The initial braking is larger than necessary to bring the sensor platform to a halt and thus the braking has to be gradually reduced as the object is approached. When the object is reached the velocity and braking will be zero resulting in a soft collision or no collision at all. This case is particularly valuable since its end conditions are favourable for many applications such as parking, docking and aircraft landing.
- 4) $k = 0.5$. Here, a constant braking is applied such that the velocity decreases linearly until the platform comes to rest at the target location.
- 5) $k > 1$. Here, the sensor system accelerates towards the target. If k is close to 1 then the acceleration comes only when the platform is close to the target. While if $k \gg 1$ the acceleration begins immediately. The resulting collision tends towards the catastrophic.

Flow fields can be coupled together [7], [13], that is to say they can be linked such that action based on one field can be directly associated with another. The coupling can be expressed by a simple linear relationship:

$$\tau_{\chi} = m\tau_{\gamma} \quad (4)$$

where τ_{χ} is the time to close a gap between the current value and a desired value of a parameter χ . In other words the parameter χ can represent, range, angle or even echo power. Equation (4) couples the flow fields of χ and γ such that both gaps must close at the same moment in time, but that the gap in χ closes m times faster than that in γ . This allows the simple example above to be easily extended to three-dimensional trajectories.

II.B Bats’ Use of Echoic Flow

As an indication of the utility of echoic flow, we consider if the species of bat, *Glossophaga soricina*, relies upon echoic flow. In their 1995 paper [6], Lee *et al.* provide a method to test whether a bat is using an echoic flow based guidance and control scheme as it approaches its prey. Here we apply their procedure to recordings of the flight trajectory of *Glossophaga soricina* as it approaches a flower to feed, and conclude that it is using echoic flow for its guidance and control.

Lee *et al.* consider that the bat could be using echoic flow for both the range and angle variables required for navigation. They consider the bat to be measuring the range to its prey, r , and the angle between its current heading and its desired direction of approach, α , from its echolocation cries. For *Glossophaga soricina*, the prey is a flower rather than an insect. Flow fields for these two variables, τ_r and τ_{α} , can therefore be defined using (1) since there are gaps between the current values and the final values and the variables are changing with time. Clearly, the bat will need the value for both flow fields to come to zero at the same time so that it has the correct heading as it arrives at the flower. There are three possible procedures the bat could employ using echoic flow to achieve this objective.

Procedure 1: Keep the values of the flow field derivatives fixed to some constant, $\dot{\tau}_r = k_r$ and $\dot{\tau}_\alpha = k_\alpha$, see discussion of (2) and (3), but treat the two fields as independent. This procedure is somewhat lacking, since once the values of k_r and k_α are set processing proceeds independently and some small error in either variable would result in the two gaps closing out of synch.

Procedure 2: Adopt α as the lead variable, fixing $\dot{\tau}_\alpha = k_\alpha$ to control the approach in angle, and then coupling the range flow field to that of angle, i.e. $\tau_r = m_{r\alpha}\tau_\alpha$. This way, as described in the discussion of (4), the gaps in both variables will close at the same time ensuring the bat arrives at the flower with the correct heading.

Procedure 3: Adopt r as the lead variable. This is the opposite of procedure 2, but now the bat has $\dot{\tau}_r = k_r$ and $\tau_\alpha = m_{\alpha r}\tau_r$.

As a result of the above three procedures there are three possible pairings of linear relationships that may be evaluated from the bat trajectory data:

- 1) $\tau_r = k_r t$ and $\tau_\alpha = k_\alpha t$
- 2) $\tau_\alpha = k_\alpha t$ and $\tau_r = m_{r\alpha}\tau_\alpha$
- 3) $\tau_r = k_r t$ and $\tau_\alpha = m_{\alpha r}\tau_r$

where t is time.

There are only three linear relationships in the list, and if any pair was to hold exactly the third would also hold and trajectory data could not be used to distinguish between the cases. However, the bat is a natural system and inevitably there will be some error. As such, Lee *et al.* propose to perform linear regressions against the extracted τ_r and τ_α as function of time and τ_r as a function of τ_α . By comparing the r^2 constant of the regression, the measure of how good the fit is, they observe that it is possible to discern between the three different procedures using the trajectory data. The discrimination criteria are defined in Table I. In all situations, the value of r^2 should be high, however, the linear regression with the lowest fit quality indicates which of the procedures is being followed.

Table I: Predicted magnitudes of r^2 if *Glossophaga soricina*, were following a particular procedure.

Procedure	Linear Regression r^2 value for		
	τ_α vs τ_r	τ_r vs t	τ_α vs t
1	Lowest	High	High
2	High	Lowest	High
3	High	High	Lowest

The 3D trajectory of the bat approaching a flower is show in Fig. 2(a). It can be seen that the bat flies in a loop around the flower. In line with the procedure described in [6] here we only consider a 2D projection of the trajectory, that is shown in Fig. 2 (b), and is the projection into the y - z plane. In addition to the projection, in Fig. 2(b), a 3 tap Butterworth filter, with a 6 Hz cutoff, has been used to high pass filter the data and remove small oscillations in the position associated with the beating of its wings.



Fig. 2: The trajectory of *Glossophaga soricina* bat approaching a flower to feed (a) in 3D and (b) 2D with smoothing applied.

The data is further pre-processed from Fig. 2(b) before undertaking the echoic flow analysis. First, the final 50 ms of data is omitted. Bats tend to twist their bodies at the moment they connect with the flower so the motion in these final moments would not be expected to follow the echoic flow guidance and control. Second, only the 300 ms of data leading up to the final 50 ms are included in the analysis, since the control constants k_α , k_r , $m_{r\alpha}$ and $m_{\alpha r}$ must vary over extended time scales as the bat undertakes different activities. Third, and finally, a quadratic fit is made to the data being processed to remove any data recording errors. The final data, against which the echoic flow regression analysis is undertaken, is shown in Fig. 3. The black dots are the original data, after application of the Butterworth filter, the blue line is the quadratic fit to the data and the dashed red line indicates the final direction. The r^2 value of the quadratic fit is 1 to two decimal places indicating an excellent fit. The range, r , to the flower is the straight-line distance between the points along the blue line and the flower. The angle α is angle between the bat's current heading direction and the dashed red line.

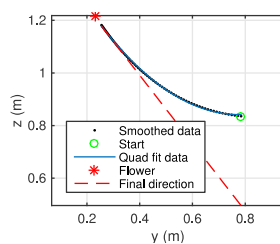


Fig. 3: The bat trajectory data upon which the echoic flow regression analysis is made.

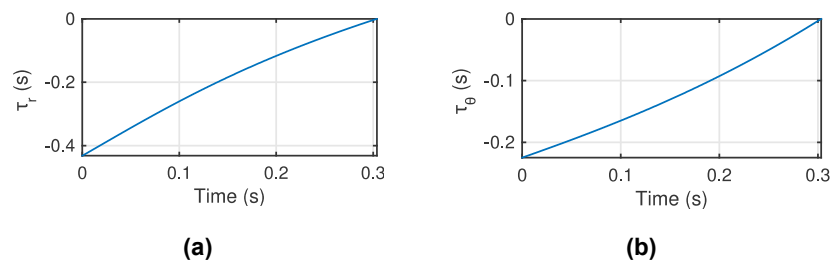


Fig. 4: Echoic flow as a function of time for (a) range to target, r , and (b) angle between current and desired heading, α .

The curves of the range and angle echoic flow are presented in Fig. 4. A visual inspection of the two curves showed them to deviate slightly from straight lines. However, when a linear regression was applied the r^2 values for a $y = mx + c$ fit were found to be 0.93 and 0.94 for τ_r and τ_α respectively. For the plot of τ_r as a function of τ_α the value of r^2 was 0.97. All of these r^2 values are high, so we may conclude that the linear regressions are good. Further, from Table I we may conclude that *Glossophaga soricina* is following procedure 2 in which the angle, α , is the lead variable and the range, r , is coupled to it through echoic flow theory.

More generally, we might conclude that the presented analysis and results provide evidence that *Glossophaga soricina* does use echoic flow for its guidance and control as it approaches flowers to feed. This conclusion strengthens the arguments for use of echoic flow in cognitive radar, since we have now seen a biological example and we may assume that through the process of natural selection the bat's behaviour is optimal. Now that we have an appreciation of how *Glossophaga soricina* controls its flight trajectory, our attention turns to how it conducts the discrimination of the flower it wishes to feed from background clutter.

II.C Echoic Flow Experiments

II.C.i Robotic Guidance and Control Experiments

We seek to develop a cognitive guidance methodology that will enable an autonomous vehicle or robot to avoid collisions. At the heart of a cognitive architecture is the perception-action cycle [2]. Within the cycle sensors provides input data that is converted into a perception i.e. a representation of the local environment. Rules, representing the experience and learnt behaviour of humans, are then applied to the perception to decide upon actions. Memory is required to facilitate the decision making process and may be divided into two parts: first, short term memory that stores values as the sensors measurements; and second, long term memory that stores the rules and control constants pertinent to the current task. The execution of the actions change the relationship between the robot and the environment that in turn changes the perception and the cycle continues. By developing an appropriate perception and the sets of actions and rules cognitive guidance may be performed.

In [4], [5] the concept of using EF for cognitive guidance was demonstrated using a simulation. A robot platform was hypothesised that had a dual beam monostatic radar mounted on the front, see Fig. 5(a), that observed the environment at $\theta = \pm 45^\circ$ to the direction of travel. The EF was calculated in each beam and the robot turned away from the direction with lowest flow. Despite the simplicity of the approach the simulated robot was able to successfully traverse corners and avoid obstacles.

The simulated results have been repeated experimentally [14]. The implementation of the robotic platform is shown in Fig. 5(b). The platform uses ultrasonic sensor to measure range, a replacement for the radar hypothesized in [4], [5] but still echoic sensors. The platform has eight sensors, but only two are used, those with $\theta = \pm 50^\circ$ to be consistent with the early simulation. In addition to measuring the ranges to obstacles, the platform also measures its speed. The measured speed is then projected onto the beam directions as $v_{l,r} = v \cos \theta$ where l and r indicate left and right to allow the EF to be calculated.



Fig. 5: The robot platform (a) schematic and (b) actual platform using ultrasonic transducers to measure range.

The perception-action cycle used to guide the robot is shown schematically in Fig. 6 with the parameters for EF mapped onto it. This cycle represents a refinement of the simple algorithm used in [4], [5] providing the robot with a more cognitive sensing architecture. The inputs to the cycle are the parameters measured by the robot

platform sensors and the outputs are turning instructions that set the rate of turning and the duration of turn. After projection of the speed onto the directions of the radar beams, the inputs to the cycle are the ranges, r_n , and speeds, v_n , for the left and right beam directions where n is the observation index. The values are stored in the short term memory and are used to calculate the EF in the left and right directions, τ_{left} and τ_{right} respectively, using (1). These two EF estimates are considered the robot’s perception of the local environment.

The selection of an action, based on the perception, requires a task objective to be known. In this research, the task was collision avoidance, and the strategy to achieve this was chosen to be, “steer away from the direction with shortest time to collision, i.e. minimum EF”. As described in [4], [5], if an infinitely long straight corridor were imagined, this strategy would steer onto the centre line and so achieve the task of not colliding. Based on the perception, a set of three rules was identified. The rules are listed in Table II.

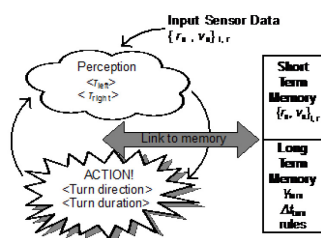


Fig. 6: Guidance by echoic flow performed by a perception-action cycle.

Table II: Rules for cognitive guidance by echoic flow.

Rule ID	Rule
1	If $\tau_l > \tau_r$ then turn right
2	If $\tau_l < \tau_r$ then turn left
3	If performing a turn set the duration of the turn to be $\Delta t_{\text{turn}} = f(\tau_l - \tau_r)$

For rules, 1 and 2 it should be noted that the sign convention of (1) produces a negative echoic flow for closing gaps, so $\tau_l > \tau_r$ indicates the shortest time to collision is too the left and a need to turn right. Rule 3 depends on the function $f(\cdot)$ that determines the turn duration. It was defined as:

$$\Delta t_{\text{turn}} = f(x) = \begin{cases} 0.4 & \text{if } x > 4 \\ \frac{x}{10} & \text{if } x \leq 4 \\ 0 & \text{if } x = 0 \end{cases} \quad (5)$$

where $x = |\tau_l - \tau_r|$. Equation (5) says that if the flows to the left and right are equal, $x = 0$, then the duration of the turn is 0 s and the robot continues straight forward; if the difference in flows is larger than 4 s then the duration of the turn is capped at 0.4 s; and for the in between cases the duration of the turn is one tenth the difference in the flows.

The rule is somewhat empirical and was developed in the laboratory by experimenting with the available robotic platform. As discussed below, the robot does not have a fully functioning radar, rather a set of ultrasonic range measures that may be used to simulate one. Equation (5) accounts for the slow repetition rate of these sensors as well as other limitations of the platform. Current research involves developing ultrasound radars to provide superior performance that will change the nature of (5).

The cognitive guidance approach described above was implemented on an Adept MobileRobots Inc. Pioneer 3-DX platform, as shown in Fig. 5(b). As noted above the robot platform is equipped with eight SensComp Series 600 ultrasonic range measurement devices. These replace the radar system hypothesized in the original simulation work. They have a transmission frequency of 50 kHz and can measure to a maximum range of 10.7 m with a stated ranging accuracy of 0.1%, although the Adept MobileRobotics interface software limits the maximum range to 5 m. The PRF of a single sensor in the robots array is 3 Hz. Each has a beamwidth of 20°. The robot platform is connected via a serial cable to a laptop that runs the interface software and allows implementation of the cognitive guidance algorithms in MATLAB. Throughout the experiments the speed of the robot was set to be 0.1 ms^{-1} , unless otherwise stated.

Experimental Trials

The robot platform was placed in an environment made from plywood walls lined with corrugated packing card. Each section of wall was 1 m long and 0.5 m tall, with feet on the rear to allow it to stand. By arranging the wall sections, different corridors for the robot to move in could be created. The corrugated packing card gave a rough surface that ensured range measurements could be made at oblique angles.

Long Straight Corridor

For the first experiment, the robot was placed in a long straight corridor of 2 m width. The robot was placed off-centre with its forward direction at 50° to the corridor centre line. The path followed by the robot is shown in Fig. 7. The thinner black lines indicate the corridor walls, and the thicker red line indicates the path followed by the robot. Initially, the robot turned sharply to its right to avoid the nearby wall. It then proceeded towards the centre line gradually reducing the angle between its forward direction and the centre line. Also visible on the path are some small oscillations.

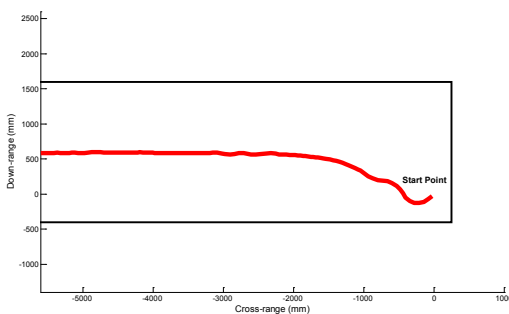


Fig. 7: Path followed by robot in long straight corridor.

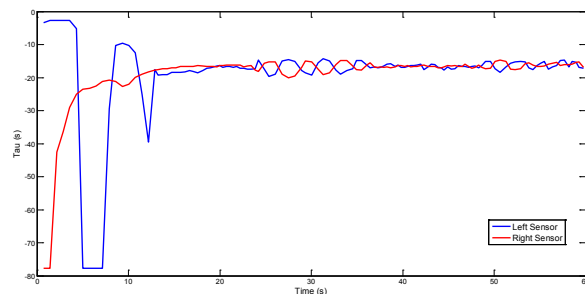


Fig. 8: Robot perception for the straight corridor experiment.

The robot's perception, the echoic flow in the left and right facing sensors, is shown in Fig. 8 as a function of time. The blue line is for the left sensor measurement; the red, the right. The sign convention of (1) causes the EF to be negative for each sensor. At times $t < 1$ the right EF remained fixed at -78 s . This was because the right sensor pointed along the length of the corridor and so measured the maximum range of 5 m. Combined with the fixed velocity, this situation provided a lower limit on perception. The left sensor pointed towards the nearby wall and measured an EF value close to 0 s. The initial perception caused the robot to turn hard right, as can be seen in Fig. 7. The robot actually turned so far to the right that the left sensor pointed along the length of the corridor and right towards the right hand wall. This can be seen in Fig. 8 when $8 < t < 9$ and the left

sensor's echoic flow was at the minimum value. From $t = 9$ onwards the path of the robot was smooth as it made its way onto the centre line.

At $t = 23$ there was a clear oscillation in the left and right echoic flows. This corresponded to the oscillation in the path visible in Fig. 7 at a cross range of ≈ -2300 mm. The origin of the oscillation is not known. However, it is thought that it relates to a discontinuity in the corridor surface that caused the ultrasonic sensor to measure the range to the discontinuity rather than the centre of the beam's footprint on the wall. This anomalous measurement caused a misperception of the EF and the robot to turn off of the correct path. It is important to note that despite this error the cognitive guidance algorithm quickly corrects itself.

Guidance in a Square Corridor

For the second experiment, the robot was placed in a square corridor with a 1 m width. In this instance the robot was placed on the centre line, facing along the corridor, and its speed increased to 0.25ms^{-1} . The path followed by the robot is shown in Fig. 9. The robot traversed the corridor in a clockwise position, starting at (0, 0). It is clear that without changing the cognitive guidance the robot is successfully able to turn the corners.

The perception for the square corridor case is shown in Fig. 10. Initially the two EF measurements were similar and the robot followed a straight-ahead path. At the first corner, once the right sensor observation passed the apex the right EF fell dramatically, and the robot turned right. As it turned the right sensor momentarily picked up the apex again, causing the sudden rise in the right EF at $t = 7$. This pattern was repeated at two of the remaining corners, while at the remaining corner the apex was not re-observed. This difference between the corners is indicative of using a cognitive rather than deterministic guidance rule.

The cognitive approach to guidance here is highly dependent on the relationship between the robotic platform and the environment. As such even slight differences in perception cause different paths to be followed. The robot was left to complete five laps of the square corridor and the path followed is shown in Fig. 11. It is clear that no two laps were the same, nor were any two corners traversed in quite the same way. We might compare this with a person reversing a car out of a driveway. Even if they do it every single day, the path followed will always be slight different.

Square Corridor With Obstacles

For the final experiment, a series of chicanes were added to one side of the square corridor. The robot started on the centre line of the corridor, but its forward direction was rotated 65° to the left. The reduction in speed was necessary because of the low PRF of the ultrasonic sensors. The robot must wait $\frac{1}{3}$ s for an update in the range measurement. In this time it continues to move forwards. For the tighter maneuvering needed in this test slowing the robot was necessary. If the sensors provided a faster update rate, it is postulated that the robot would be able to traverse this course at the same speed as the others.

The path followed by the robot is presented in Fig. 12. It is clear that the robot quickly navigated onto the centre line and traversed both the corners and obstacles successfully. The red line, that indicates the robots path in Fig. 12, comes very close to the second obstacle but there was no collision. Again, it is postulated that with an increased PRF the performance would have been better through the obstacles.

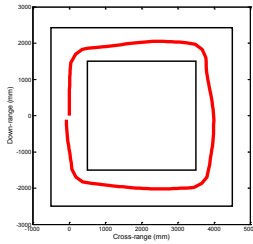


Fig. 9: Path followed by robot in the square corridor.

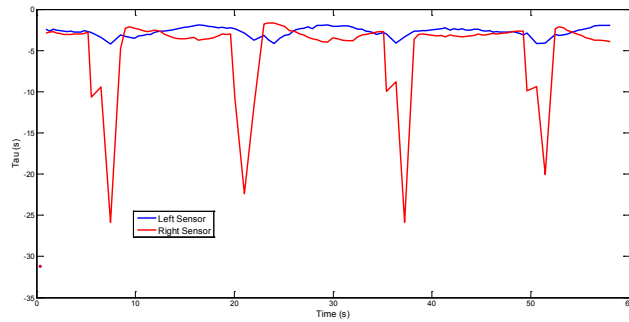


Fig. 10: Robot perception for the square corridor experiment.

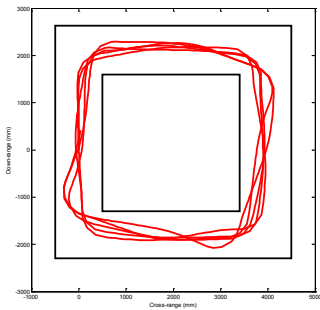


Fig. 11: Variations in path followed by robot.

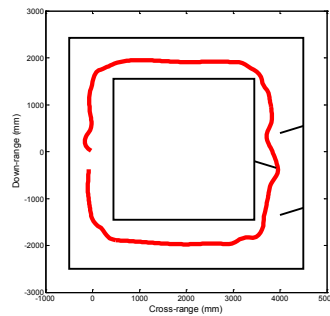


Fig. 12: Path followed by robot in the square corridor with obstacles.

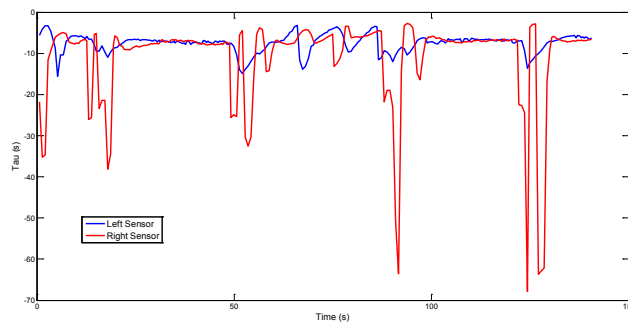


Fig. 13: Robot perception for the square corridor with obstacles experiment.

The robot's perception, as a function of time, is shown in Fig. 13. For $t < 4$ the right EF was the smaller as the robot turned away from the wall it faced at the start of the experiment. At $t = 12.5$ the robot began to navigate the first corner. The change in perception as it traversed the corner was similar to, but more extreme than, the corner case analyzed above. The additional fluctuations here arose because the initial conditions for the test prevented the robot being on the optimal centre line as it entered the first corner. The perception through the second corner, starting at $t = 49$ was the comparable to the case analyzed above since the starting effects had been forgotten. However, as soon as the robot exited the corner it perceived the obstacles, and the EFs between

50 s and 100 s varied rapidly as the robot traversed the obstacles and the third corner. Again, the perception at the fourth corner was different to the simple square corridor corner cases because the obstacles affected the exit from the third corner and the length of the section was not sufficient to get onto the centre path and aligned with the corridor direction.

II.C.ii Tau-dot Experimental Results

The robot described above in Section II.C.i was used in an experiment to validate the use of tau-dot for acceleration/braking control. In this test the forward facing range sensor was used to measure distance—essentially, estimate the gap size—and then the deceleration necessary to stop calculated by rearranging (2) for \ddot{r} .

The experimental setup at time 0 s is shown in Fig. 14. The robot starts a distance 5 m from a wall with a velocity of 0.5 ms^{-1} towards the wall. Every time the robot makes a measurement of the range to the wall, 1 m is subtracted from it prior to processing. This has the effect of moving changing the wall location in the robot's perception of the environment, moving it closer, so the robot will stop early—at the location indicated by a dashed line in Fig. 14. This offset was included to prevent the robot crashing. After each measurement of the range, the acceleration is calculated from (2) and from this a new velocity setting made according to $v' = v + a\Delta t$ where v' and v are the new velocity and current velocity respectively, a is the calculated acceleration (negative for braking) and Δt the time interval. In this experiment $\Delta t = 0.35 \text{ s}$.

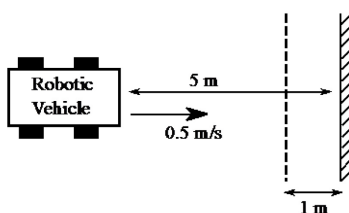


Fig. 14: Experiment setup to validate tau based equations of motion curves.

The results of the experiment for differing fixed values of $\dot{\tau} = k$ are shown in Fig. 15. This figure is an experimental version of Fig. 1 and the same colours are used to indicate the different k values. A visual comparison shows a very strong similarity between the theoretical and experimental curves. Some slight deviations are visible in the curves. This primarily takes the form of visible noise and the $k = 0.5$ acceleration line (black) not being flat. The deviations from the theory were attributed to three factors: \dot{r} was taken to be the velocity value passed to the robot control hardware and did not allow for any error in the gearing or wheel slip; at low speeds the robot was observed to have somewhat jerky motion; and no consideration was given to how long it took the robot to change its speed once a new speed instruction was issued. The sudden drop in acceleration for the $k = 0.5$ case at the end of the experiment arises because the robot slightly overshot the stopping point. Under these conditions there is a sudden change in sign for the gap size that is not accounted for in the processing.

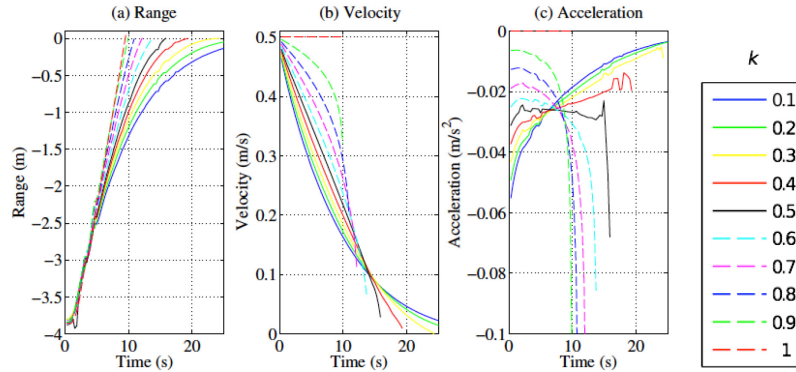


Fig. 15: Experimental curves of motion for various tau-dot values

Despite the slight limitations, it was clear that the tau-dot based control rule could govern system braking. It is of note the translation from the theory of Section II.A to the experiments was particularly straightforward. Equation (2) was used in the form it is presented in this manuscript to obtain the required deceleration and this was in turn used to calculate the required velocity by Newtonian equations. No filtering or conditioning of the sensor data was required. As such, this simple experiment goes a long way to demonstrating that echoic flow is a natural domain for guidance and control activities and has potential as the correct way to frame the activity to support cognition.

II.C.iii Target Interception Simulation

A cognitive radar system can measure range, r , and angle, θ , accurately and through (4) couples the flow fields as $\tau_r = m\tau_\theta$ so that the range and angle gaps close at the same time. Consider the example of a radar sensor (on a vehicle) intercepting a moving target following a non-ballistic, or irregular trajectory. The radar sensor measures the range, r , and angle, θ , to the target on a pulse-by-pulse basis. Over two pulses the radar is therefore able to perceive the flow field for the parameters as:

$$\tau_\chi = \chi_n / (\chi_n - \chi_{n-1}) \quad (6)$$

where χ is either r or θ and n is the pulse number.

Replacing r with χ in (6), to indicate application of the equation to a general parameter, and re-arranging gives an expression for the acceleration:

$$\ddot{\chi} = \dot{\chi}^2 (1 - \dot{\tau}_\chi) / \chi \quad (7)$$

This is the acceleration required, based on the current time to collision, to close the gap in the parameter χ . During the action phase of the cycle the radar sets the linear and angular accelerations of the platform to the values obtained from (7). This is repeated every pulse from the second pulse allowing control of the platform velocity and heading direction.

Fig. 16 shows a platform being guided by a radar that processes echoic flow intercepting an accelerating target. The radar is capable of perceiving the flow in the x and y directions based on its measurements of range and angle. The decision to use the x and y directions rather than range and angle is for ease of simulation implementation and not to suggest they are preferable. The two fields are coupled and through (4) and (7)

updates to the platform acceleration can be calculated from each radar pulse to guide the platform to the target. The initial velocity of the sensor is 20 ms^{-1} with a heading angle of 45° , measured from the y direction. The acceleration is set to 0 ms^{-2} and is along the heading direction. The target location is 250 m from initial platform position and the angle between the line of sight (LOS) and the heading direction is 20° . The target will be assumed to have an initial velocity of $\mathbf{v}_{tgt} = 10 \times [\sin 20 \quad \cos 20]^T \text{ ms}^{-1}$ and an acceleration of $\mathbf{a}_{tgt} = -0.5 \times [0 \quad 1]^T \text{ ms}^{-2}$. At the end of the simulation, the final target velocity was $[3.4 \quad -5.6]^T \text{ ms}^{-1}$ while the platform final velocity vector was $[3.6 \quad -5.5]^T \text{ ms}^{-1}$. The absolute error between the two velocities is small, just 0.2 ms^{-1} .

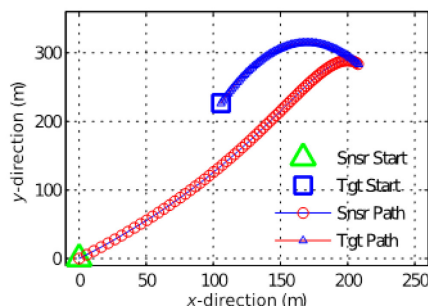


Fig. 16: Interception of a moving target. The guidance and control of the sensor platform is achieved using the echoic flow measured in the x and y directions and the two flow fields are coupled.

This example of guidance and control demonstrates how, when the right perception is taken from the radar data, i.e. echoic flow, actions can be decided on easily. Here, the action is to correctly set the vector acceleration such that the target is intercepted and its heading and speed are matched. The acceleration is calculated (action decided on) using (7), with the distances to the target in the x and y directions substituted in for χ , and (6) resulting in a deterministic implementation of the perception-action cycle. The cycle is normally considered to act in the presence of memory; here we might consider the memory to be the fixed value of $\dot{\tau}$ required in (2) and (6) and the value of m from (2). The system remembers which value of $\dot{\tau}$ and m to use, 0.5 and 2.14 , respectively, in the example, to obtain a desired approach trajectory.

Echoic flow based cognitive guidance and control has many applications in the real world. One example would be a landing aid for a helicopter approaching the helipad on a ship. The ship is moving in the sea, so even if the helicopter remained stationary, the range would vary. If the helicopter is descending, (7) provides a deterministic implementation of the perception-action cycle in which the required action—braking (\ddot{r} , substituted in for $\ddot{\chi}$ in (7))—can be determined based on the perception or measurement of echoic flow. Since the echoic flow perception is time varying, the motion of the helipad merely changes the instantaneous estimation of the flow and the braking action automatically adjusts such that the landing type, determined by the control constant, k , will still occur. As a more sophisticated example, if the target in Fig. 16 were considered to be a space in a line of moving traffic then it is clear that echoic flow could be used to allow a self guiding car to merge in. Clearly echoic flow has many potential applications and is a demonstration of the power of cognition coupled with radar sensing.

III EXPERIMENTAL DEMONSTRATION OF COGNITIVE PROCESSING

Current radar design approaches use a fixed set of parameters, largely driven by a requirement to achieve a pre-determined signal to interference plus noise ratio (SINR) at the maximum desired operating range. The design

then proceeds against assumed target and clutter models that represent average anticipated responses. Variations in target type, target reflectivity, clutter and other environmental factors all combine such that the desired performance is only achieved on average and hence there are periods where substantial shortfalls occur. Further, this traditional design approach means that the radar performance is often over specified for some operations—such as tracking short range targets, for example, when shorter coherent processing intervals (CPIs) might be used to obtain an acceptable SNR—resulting in unnecessary use of valuable resources and consequently suboptimum use of the radar timeline. This is especially important in electronically scanned array radar systems where tracking of targets can absorb the whole of the radar timeline, interrupting surveillance and causing potentially important targets to escape detection. Additionally, traditional radar designs make little use of parametric feedback in performance optimization. Traditional single target tracking radars come the closest where the aim is to maintain the target at the centre of the beam. However, such systems only make use of a fixed parameter set, the selection of which is, again, largely dictated by a desired maximum operating range.

This paper presents experimental results from a cognitive radar that demonstrates its superior performance and shows how this can be realized in a relatively easy and straightforward fashion. This research has been conducted within the Cognitive Sensing Laboratory at The Ohio State University (OSU) ElectroScience Lab, in conjunction with the Air Force Research Laboratory and Metron, Inc.

III.A Experimental Setup

III.A.i The CREW

The Cognitive Radar Engineering Workspace or CREW is a mm-wavelength, four transmit and receive channel, multistatic radar system with a real-time adaptation capability. The system uses four arbitrary waveform generators to produce any desired waveforms for any transmit channel. These baseband waveforms are then up converted to an IF frequency using a baseband converter module. The IF signals are distributed, along with a second LO signal that can vary around 16.5 GHz, to four transmitter heads that frequency multiply the LO signal and then up-converts the IF signal to W-band for transmission. The second LO frequency can be stepped from pulse to pulse to provide a total operational bandwidth of 4 GHz. The received signals are down-converted inside the four receiver heads and the resulting IF signal is then shifted to baseband in the baseband converter module. The baseband signals are then digitized using four ADCs that are controlled via a PC. Table III shows the principle operating parameters. Polarization diversity is via manual rotation of the RF heads and can only be done on an experiment-to-experiment basis.

III.A.ii Cognitive Processing Architecture

The cognitive architecture implemented is an instantiation of the framework proposed in [15], [16] this time being used to control the PRF and number of pulses per CPI such that a target tracking error is met. A reduced complexity version of this framework instantiation is given in [17], where only one parameter is adapted rather than the two parameters considered here.

The cognitive radar tracking is based on a *maximum a posteriori penalty function* (MAP-PF) tracking methodology, which allows cognitive control of both the radar sensor and the processor. Here MAP-PF is used to demonstrate the cognitive performance improvements possible when combined with the CREW system. The cognitive processing algorithm executing on CREW allows the PRF to be adjusted to optimize tracking performance, while keeping the target from being Doppler-aliased and away from the zero-Doppler clutter. The CREW also allows the number of pulses integrated each CPI to be adapted so that the signal to interference and noise ratio (SINR) can be kept above a minimum pre-prescribed value.

III.A.iii Experimental Setup

A single channel of the CREW, that is one tx head and one rx head, was used for this experiment. The tx head was mounted for vertical polarization; the rx head, horizontal. The use of cross-polarisation had been found in previous, informal testing to improve the signal to clutter ratio. The two heads were placed in a corner of the laboratory at a height of approximately 1.5 m. A volunteer from the experimental team was used as a target, and the volunteer walked backwards and forwards in front of the radar between 1 m and 8 m of range.

Table III: Operating Parameters of the CREW.

Parameter	Value
Max Tx power	25 dBm
Frequency range	92 - 96 GHz
Pulse Width	1ns to 100 μ s
PRF	Up to 30 kHz
Waveform	Programmable pulse to pulse
Number of transmitters	4
Antenna gain (Tx & Rx)	33 dB
Antenna beamwidth	2°
Number of receivers	4
A/D – Keysight M9703A	Four 3.2 Gs/s 12 bits channels
Waveform generation – Keysight M8190A	12/14 bit resolution at 8Gs/s (14 bit) or 12 Gs/s (12 bit) and an SFDR of 90 dBc
Baseband convertor	Input freqs: 0.3 – 1.3 GHz Output freq: 5 – 6 GHz Transmit gain, 20 dB and noise figure 19 dB Receive gain, 12 dB and noise figure 5 dB

The CREW ran an extension of the MATLAB code developed for the “after the fact” cognitive processing of experimental data described in [17]. The extension was to add optimization of the number of pulses in a CPI. With the tracker, the SNR is considered part of the target state vector. Once the appropriate PRF has been selected based on the prediction of the target state at the next time interval, the number of pulses in the CPI is set to ensure the SNR is above a predetermined level, since sufficient SNR is essential for low tracking error.

For the initial tests, the adaption parts of the cognitive processing architecture were disabled and the system operated with PRFs of 6, 4 and 2kHz. The number of pulses in a CPI was fixed at 128. For the adaptive tests, initially the PRF was permitted to vary, and then in a further test that moved beyond [17] adaption of the number of pulses per CPI was included such that the SINR was kept above 15 dB.

III.B Discussion of Results

In all results the change in SINR as a function of target range was clearly visible. However, it was also observed that the orientation of the volunteer’s body also caused significant SINR variation.

In the first experiment the PRF was fixed at a value of 6 kHz. Fig. 17 shows the output results after running the experiment. The range, velocity and the SNR track plots all show the mean and two-sigma error of the predicted values along with the actual measurements. The normalized Doppler frequency (normalized to the PRF) plot shows upper and lower bounds set for the PRF along with the maximum predicted and mean target Doppler values. The velocity and range standard deviation plots show the root mean squares of the predicted and posterior tracker values as a function of elapsed time. The dotted line indicates the performance goal. Below that are the time elapsed plots for the PRF and number of pulses per CPI which, in this first case, are fixed.

The high PRF value resulted in the measurement and tracking processes not becoming ambiguous. This was indicated by the magenta curve on the normalized Doppler frequency graph remaining below the upper bound. However, the high PRF also caused Doppler filter bin widths wider than would be ideal to control the velocity errors and the predicted velocity error significantly exceeded the error goal on two occasions. Additionally, fluctuations in the SINR caused the range error to similarly miss its goal. The degree of error in range was observed to be fairly direct function of SINR. Overall, this would be deemed a non-optimum solution even for a traditional fixed parameter approach to radar design.

Fig. 18 shows a second experiment in which the human target undertook, as closely as possible, the same range of positions and velocities as before (as was done in all the experiments). Due to space limitations, we do not include the position and velocity tracks in the remaining plots. This time the PRF was fixed at 2 kHz. For this case, the PRF was too low to sustain unambiguous operation, although in general the reduced Doppler bin width improves the velocity error. The exception was when the SINR dropped to too low of a value. The range error was more greatly influenced by SINR and exceeded the desired goal when the SINR fell.

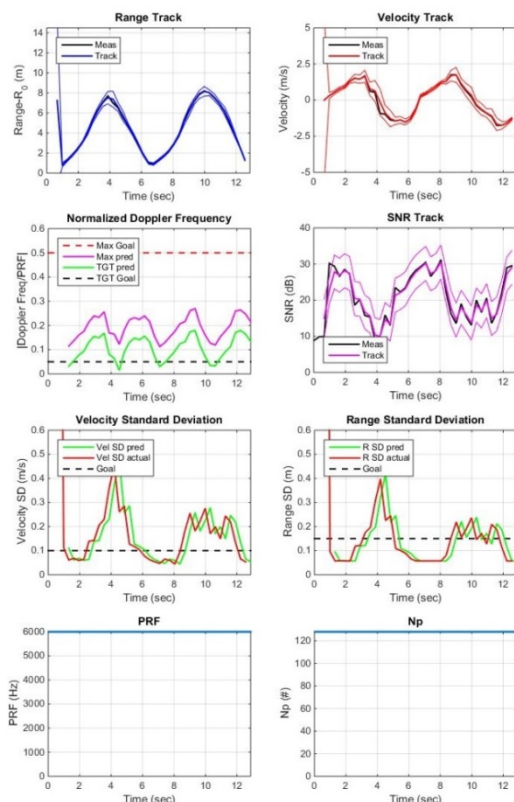


Fig. 17 Experimental results for a fixed PRF (6 kHz) and a fixed number of pulses (128) used for integration.

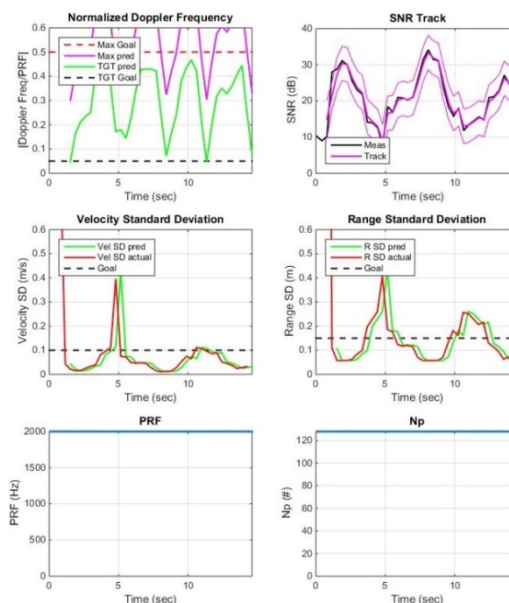


Fig. 18 Experimental results for a fixed PRF (2 kHz) and a fixed number of pulses (128) used for integration.

The 4 kHz results, not presented here, represent a compromise between those at 2 and 6 kHz. Indeed, for the PRF objectives this was the case. However, there were still periods where the velocity and range errors exceeded the desired limits. These were, again, coincident with regions where the SINR fell below approximately 15 dBs.

The PRF adaption results are shown in Fig. 19. It can be seen that the maximum predicted Doppler, as shown by the magenta trace, was always kept within the unambiguous limit. The changing PRF value can be seen directly in the bottom center figure. The driving of the PRF to the lowest possible value at any instant in time had the desired effect of controlling the velocity error so that it barely exceeded the prescribed performance level. However, there was a SINR dip between 4 and 8 seconds that had a pronounced effect on the range error causing it to rise significantly above the desired level.

The results of the final test, adapting the PRF and number of pulses, are shown in Fig. 20. This time, on the two occasions where the SINR started to fall, the number of pulses integrated is increased so that the effect on the range error as well as the velocity was controlled and the performance was very close to that prescribed. The plots showing the velocity and range errors now show a performance in velocity that is within the specified performance limit with range just exceeding it on a couple of occasions.

These results show the power of a cognitive approach to radar sensing for maintaining a desired level of tracking performance. Indeed, instead of designing a radar by specifying the system parameters and then developing

sophisticated tracking algorithms to cope with Doppler ambiguities and target fading, we are now able to design a cognitive tracking radar by specifying the performance.

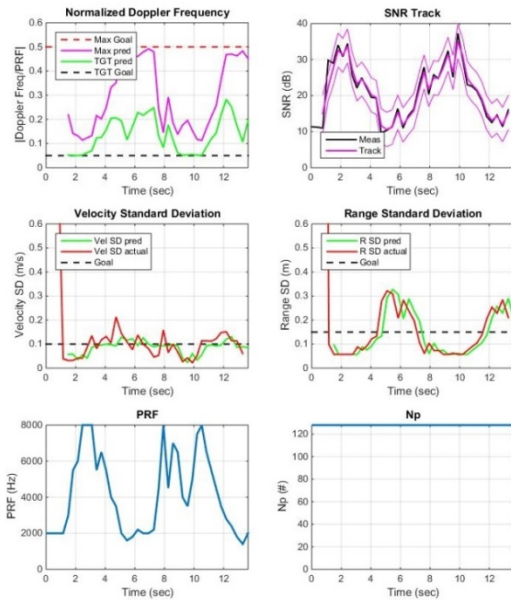


Fig. 19 Experimental results for a variable PRF and a fixed number of pulses (128) used for integration.

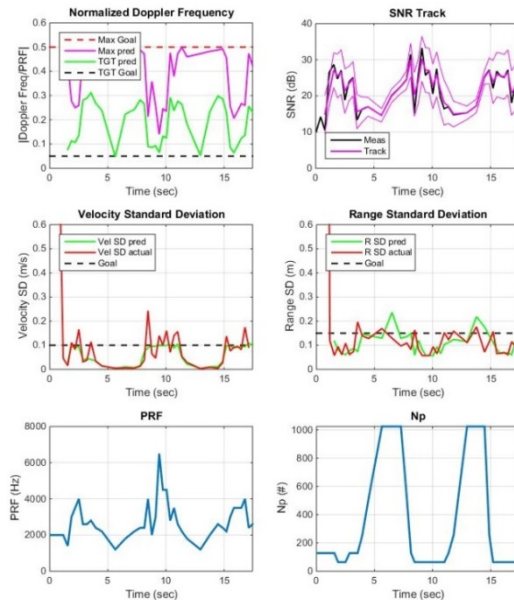


Fig. 20: Experimental results for a variable PRF and a variable number of pulses used for integration.

IV CONCLUSIONS

Echoic flow provides a mathematical framework to describe how animal cognition may perceive the input from echoic sensors, such as a bat’s ultrasonic radar. Echoic flow can be generalized to flow theory that can be used to describe the perception from other natural sensors, such as the eye, and to describe how sensory and motor neuronal responses are coupled together. The evidence for flow in the literature from biology and neurology is compelling and suggests that it is a core part of how creatures are able to build a perception, and decide actions bases upon, their sensory inputs—i.e. function as cognitive beings.

From an engineering standpoint, echoic flow provides a framing from which synthetic cognition can be developed. The theory allows the formation of perceptions that are simple enough to be represented in a computer memory. In addition, it provides methods to combine the different parts of the perception together, the tau coupling, and to convert the perceptions into actions, such as when tau-dot theory is used to develop a controlled braking strategy.

The experimental and simulated results presented demonstrate how straightforward it is to apply the theory. The robot steering experiments show that when an appropriate framing for the problem is made, cognitive like behavior can be achieved using a simple, well thought out if...then...else statement. Meanwhile the tau-dot braking results indicate how the theory can be applied directly and obtain results consistent with the analytic

solutions. Finally, the simulation that combines the tau-dot controlled acceleration in two directions provides insight into how far echoic flow based guidance and control may be taken—control of a moving vehicle in two dimensions is easy and extension to three dimensions would be a straightforward step.

In the second part of this paper the CREW has been introduced as a flexible, adaptive radar system for examining new cognitive based approaches to radar design. It has been shown, through a simple tracking demonstration, how a cognitive approach can yield superior performance when compared with the traditional fixed parameter approach. This is applicable to any type of radar and is a relatively simple and low cost extension. The detection performance of current monostatic radars could be improved as the cognitive approach allows higher sensitivity levels to be maintained. E-scan radars, which are often over specified for large targets at closer than maximum detection range, could use a cognitive approach to utilize their timeline much more efficiently by backing off parameters where echo characteristics allow. This will allow a greater number of targets to be detected and tracked than would otherwise be possible. This research, however, only scratches the surface of what might be possible using a cognitive approach to radar systems design. Overall, it has been shown that it is now possible to design directly to a desired performance requirement rather than designing a radar through fixed parameter selection and obtaining a performance dictated by clutter and target variations.

V REFERENCES

- [1] S. Haykin, *Cognitive Dynamic Systems (Perception-Action Cycle, Radar, and Radio)*. Cambridge University Press, 2012.
- [2] S. Haykin and J. M. Fuster, “On cognitive dynamic systems: Cognitive neuroscience and engineering learning from each other,” *Proc. IEEE*, vol. 102, no. 4, pp. 608–628, 2014.
- [3] C. J. Baker, G. E. Smith, A. Balleri, M. Holderied, and H. D. Griffiths, “Biomimetic Echolocation With Application to Radar and Sonar Sensing,” *Proc. IEEE*, vol. 102, no. 4, pp. 447–458, Apr. 2014.
- [4] G. E. Smith and C. J. Baker, “Echoic flow for radar and sonar,” *Electron. Lett.*, vol. 48, no. 18, pp. 1160–1161, 2012.
- [5] G. E. Smith and C. J. Baker, “Echoic Flow For Autonomous Navigation,” in *Proceedings of Radar 2012, The International Conference On Radar*, 2012.
- [6] D. N. Lee, J. A. Simmons, P. A. Saillant, and F. Bouffard, “Steering by echolocation: a paradigm of ecological acoustics,” *J. Comp. Physiol. A*, vol. 176, no. 3, pp. 347–54, Mar. 1995.
- [7] D. Lee, A. Georgopoulos, M. Clark, C. Craig, and N. Port, “Guiding contact by coupling the taus of gaps,” *Exp. Brain Res.*, vol. 139, no. 2, pp. 151–159, Jul. 2001.
- [8] D. N. Lee, B. Shaw, J. Farber, and J. Kennedy, “General Tau Theory: evolution to date,” *Perception*, vol. 38, pp. 837–859, 2009.
- [9] M. Vespe, G. Jones, and C. J. Baker, “Diversity Strategies: Lessons from Natural Systems,” in *Principles of Waveform Diversity and Design*, M. C. Wicks, E. L. Mokole, S. D. Blunt, R. S. Schneible, and V. J. Amuso, Eds. SciTech, 2010, pp. 25 – 50.
- [10] M. Vespe, G. Jones, and C. J. Baker, “Lessons for Radar [Waveform diversity in echolocating mammals],” *IEEE Signal Process. Mag.*, vol. 26, no. January 2009, pp. 65–75, 2009.

- [11] J. J. Gibson, *The Perception Of The Visual World*. Boston: Houghton Mifflin, 1950.
- [12] D. Fleet and Y. Weiss, "Optical flow estimation," in *Handbook of Mathematical Models in Computer Vision*, Springer, 2006, pp. 237–257.
- [13] G. E. Smith, C. J. Baker, and G. Li, "Coupled echoic flow for cognitive radar sensing," in *2013 IEEE Radar Conference (RadarCon13)*, 2013, pp. 1–6.
- [14] G. E. Smith, S. Alsaif, and C. J. Baker, "Echoic flow for cognitive radar guidance," in *Radar Conference, 2014 IEEE*, 2014, pp. 490–495.
- [15] K. L. Bell, C. J. Baker, G. E. Smith, J. T. Johnson, and M. Rangaswamy, "Fully adaptive radar for target tracking part I: Single target tracking," in *2014 IEEE Radar Conference*, 2014, pp. 0303–0308.
- [16] K. L. Bell, C. J. Baker, G. E. Smith, J. T. Johnson, and M. Rangaswamy, "Fully adaptive radar for target tracking part II: Target detection and track initiation," in *2014 IEEE Radar Conference*, 2014, no. 4, pp. 0309–0314.
- [17] K. L. Bell, C. J. Baker, S. Member, G. E. Smith, S. Member, J. T. Johnson, and M. Rangaswamy, "Cognitive Radar Framework for Target Detection and Tracking," *IEEE J. Sel. Top. Signal Process.*, vol. 99, no. 0, pp. 1–13, 2015.

